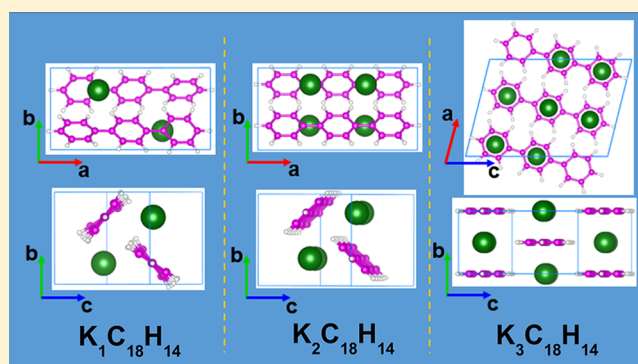


Structural and Bonding Characteristics of Potassium-Doped *p*-Terphenyl Superconductors

HPSTAR
528-2018Guo-Hua Zhong,[†] Xiao-Hui Wang,[‡] Ren-Shu Wang,[§] Jia-Xing Han,[‡] Chao Zhang,^{||} Xiao-Jia Chen,^{§,*} and Hai-Qing Lin^{‡,*}[†]Shenzhen Institutes of Advanced Technology, Chinese Academy of Sciences, Shenzhen 518055, China[‡]Beijing Computational Science Research Center, Beijing 100193, China[§]Center for High Pressure Science and Technology Advanced Research, Shanghai 201203, China^{||}Department of Physics, Yantai University, Yantai 264005, China

Supporting Information

ABSTRACT: Recently, there is a series of reports by Wang et al. on the superconductivity in K-doped *p*-terphenyl ($K_xC_{18}H_{14}$) with the transition temperatures ranging from 7 to 123 K. Identifying the structural and bonding characteristics is the key to understand the superconducting phases and the related properties. Therefore, we carried out an extensive study on the crystal structures with different doping levels and investigated the thermodynamic stability, structural, electronic, and magnetic properties by the first-principles calculations. Our calculated structures capture most features of the experimentally observed X-ray diffraction patterns. The K-doping concentration is constrained to within the range of 2–3. The obtained formation energy indicates that the system at $x = 2.5$ is more stable. The strong ionic bonding interaction is found in between K atoms and organic molecules. The charge transfer accounts for the metallic feature of the doped materials. For a small amount of charge transferred, the tilting force between the two successive benzenes drives the system to stabilize at the antiferromagnetic ground state, whereas the system exhibits nonmagnetic behavior with increasing charge transfer. The multifermionity of band structures near the Fermi level indicates that the driving force for superconductivity is complicated.



The strong ionic bonding interaction is found in between K atoms and organic molecules. The charge transfer accounts for the metallic feature of the doped materials. For a small amount of charge transferred, the tilting force between the two successive benzenes drives the system to stabilize at the antiferromagnetic ground state, whereas the system exhibits nonmagnetic behavior with increasing charge transfer. The multifermionity of band structures near the Fermi level indicates that the driving force for superconductivity is complicated.

1. INTRODUCTION

Superconducting materials have been a hot research topic in physics and materials science because of their important application values in energy, information, quantum devices, and other advanced technologies. Researchers have been devoted to the design and synthesis of new superconducting materials, the understanding of superconducting mechanism, and the exploration of superconductors with higher transition temperature (T_c). In 2010, the superconductivity of $T_c \approx 18$ K was discovered in potassium (K) metal-doped picene,¹ which opens a new avenue in the quest for organic hydrocarbon superconductors. Subsequently, the superconductivity has also been observed in alkali, alkaline-earth metals, and rare-earth elements-doped phenanthrene,^{2–5} chrysene,⁵ [6]phenacene,⁶ coronene,⁷ [7]phenacene,⁶ and 1,2;8,9-dibenzopentacene,⁸ respectively. In particular, using density functional theory and Eliashberg's theory of superconductivity, we have predicted K-doped benzene ($K_2C_6H_6$) to be superconductive with the T_c around 6.2 K and proposed that all hydrocarbons should show T_c in a similar temperature range of $5 < T_c < 7$ K under conventional conditions.⁹ The results greatly increase the

understanding of the superconductivity of polycyclic aromatic hydrocarbons (PAHs).

So far, the highest T_c reached is 33.1 K in PAH superconductors, which was obtained in K-doped 1,2;8,9-dibenzopentacene.⁸ However, previous theoretical studies showed that PAH superconductors usually exhibit the antiferromagnetic (AFM) ground state^{10–13} and exist the strong electronic correlation effects,^{13–18} indicating that the superconducting mechanism is complicated in aromatic hydrocarbons. Our theoretical predictions have argued that electronic correlations⁹ or pressure¹⁹ could enhance high T_c in aromatic hydrocarbons. Hence, organic-based compounds are candidates of high temperature or room temperature superconductors because the interaction of electrons with much higher excitation energy than the phonon energy can result in a substantially higher T_c in these low-dimensional materials.^{20,21} Thus, the higher T_c can be expected in this kind of aromatic hydrocarbons.

Received: December 22, 2017

Revised: January 29, 2018

Published: February 1, 2018

Recently, *p*-terphenyl ($C_{18}H_{14}$), a hydrocarbon compound containing three benzene rings connected by C–C bonding, draws a lot of attention. Different from the feature of sharing armchair edge in PAHs such as phenanthrene, chrysene, picene, coronene, and 1,2;8,9-dibenzopentacene, benzene rings are connected by the single C–C bond in the *p*-terphenyl molecule. Namely, *p*-terphenyl is a non-polycyclic aromatic hydrocarbon. With regard to the study of superconductivity of this system, Wang et al. claimed the superconductivity of 7.2 K in the synthesized $K_xC_{18}H_{14}$.²² Later, Wang et al. claimed to observe a higher T_c of 43 K²³ and even 123 K²⁴ in the K-doped *p*-terphenyl. They also ruled out the possibilities of the formation of K-doped C_{60} and graphite, as suggested previously.²⁵ By using high-resolution photoemission spectroscopy on potassium surface-doped *p*-terphenyl crystals, Li et al. presented the spectroscopic evidence for pairing gaps at the surfaces of these materials, with the gaps persisting to 60 K or above.²⁶ Furthermore, Liu et al. observed the superconductivity such as transition at about 125 K in their fabricated potassium-doped *p*-terphenyl with the help of magnetization measurements.²⁷ These subsequent works greatly promote the study to superconductivity of the material. However, the doping level and superconducting phases with different T_c have not been determined yet, not to mention the desired pairing mechanism. Therefore, identifying the structures and chemical bonds is crucial to the understanding of the superconducting phases as well as superconductivity, which is the focus of the current study.

p-Terphenyl has twisting degrees of freedom around the long molecular axis, which will result in complicated situations when K atoms are doped into *p*-terphenyl crystal. It has been well-known that crystallized *p*-terphenyl exhibits two phases with the variation of temperature of $P2_1/c$ symmetry at room temperature and $P\bar{1}$ symmetry below 193 K.^{28,29} In addition, the pressure also drives a transition from C_2 to D_{2h} symmetry around 1.3 GPa.³⁰ In this work, we will investigate the K doping effects on structural, electronic, and magnetic properties in *p*-terphenyl at ambient pressure by the first-principles calculations. The obtained structures will be compared with the experiments. The details for the structural and bonding features will be provided. These results are helpful for the determination of the doping level and thermodynamically stable phases as well as the understanding of the charge-transfer process and mechanism in these newly discovered superconductors.

2. COMPUTATIONAL METHOD

To study the structural and electronic properties of $K_xC_{18}H_{14}$, we employed the Vienna ab initio simulation package^{31,32} based on the projector-augmented wave method. For the plane-wave basis-set expansion, an energy cutoff of 600 eV was adopted. The Monkhorst–Pack *k*-point grids are generated according to the specified *k*-point separation of 0.02 \AA^{-1} , and the convergence thresholds are set as 10^{-6} eV in energy and 10^{-3} eV/Å in force. The generalized gradient form (GGA) of the exchange–correlation functional (Perdew–Burke–Ernzerhof 96) was adopted.³³ In addition, considering the nonlocal interaction, we have added the correction of van der Waals (vdW) in the version of vdW-DF2 in this calculation.³⁴ The necessity of vdW-DF2 functional has been confirmed by our previous studies.^{35,36}

3. RESULTS AND DISCUSSION

3.1. Determining Functional. Starting from the pristine $C_{18}H_{14}$, we first optimized the crystal lattice parameters of solid $C_{18}H_{14}$ with the $P2_1/c$ symmetry to test the feasibility of vdW-DF2 functional. The obtained crystal lattice parameters from vdW-DF2 functional are $a = 13.569 \text{ \AA}$, $b = 5.542 \text{ \AA}$, and $c = 7.911 \text{ \AA}$ and the angle $\beta = 92.8^\circ$, respectively. As seen from the crystal lattice parameters listed in Table 1, the vdW-DF2

Table 1. Optimized Crystal Lattice Constants a , b , c , the Angle β between Two Axes and the Volume of Unit Cell V of Pristine $C_{18}H_{14}$ Compared with the Experimental Values

method	a (Å)	b (Å)	c (Å)	β (°)	V (Å ³)
expt. ^a	13.613	5.613	8.106	92	619
expt. ^b	13.621	5.613	8.116	92.01	621.1
expt. ^c	13.59	5.59	8.08	92.9	613.4
expt. ^d	13.58	5.58	8.02	92.10	607.3
expt. ^e	13.55	5.63	8.15	92.60	621.1
vdW-DF2	13.569	5.542	7.911	92.8	594.2
LDA	13.215	5.292	7.443	93.57	519.6
GGA	13.596	6.283	8.574	88.89	732.2

^aReference 37. ^bReference 38. ^cReference 39. ^dReference 40. ^eReference 41.

functional products of the lattice constants are in good agreement with experimental ones, although the small difference exists among those reported experimental observations.^{37–41} The error is respectively controlled within 2.5% for the lattice constant and 4% for the volume of unit cell. However, GGA and local density approximation (LDA)⁴² functional extremely overestimates and underestimates the lattice constants (the volume of unit cell). The result indicates that the nonlocal interaction should not be ignored in this aromatic hydrocarbon. As shown in Figure 1, the calculated X-ray diffraction (XRD) spectrum of solid $C_{18}H_{14}$ shown in Figure 1 fits the experiment carried out by Wang et al.²² Additionally, the average value of carbon–carbon bond lengths within the rings is about 1.40 Å and those between rings are about 1.49 Å, which are also consistent with the experimental values.²⁹

3.2. Structure of $K_xC_{18}H_{14}$. Within the framework of the vdW-DF2 functional, we simulated K-doped *p*-terphenyl, and first considered three possible concentrations of $x = 1, 2,$ and 3 in $K_xC_{18}H_{14}$. The total energy calculation indicates that doping results in the phase transition of crystal structure. Both $K_1C_{18}H_{14}$ and $K_2C_{18}H_{14}$ are stabilized at $P2_1$ symmetry instead of $P2_1/c$. However, $K_3C_{18}H_{14}$ can exist in the form of $P2_1/c$ symmetry. The crystal lattice parameters at three doping levels are summarized in Table 2. We found that the variation of crystal lattice parameters is complicated after doping. The intercalation of K atoms leads to the obvious expansion in b direction, and the big contraction in c direction in $K_1C_{18}H_{14}$ and $K_2C_{18}H_{14}$. $K_3C_{18}H_{14}$ is abnormal because it expands in a and c directions, whereas it contracts in the b direction. However, the doping makes the system volume increase. Figure 2 clearly shows the characteristics of $K_xC_{18}H_{14}$ viewed from different directions. For $K_1C_{18}H_{14}$, as shown in Figure 2a, the herringbone structure is formed, and the K atom is between two organic molecular layers when viewing along the a direction, similar to K-doped picene¹ and phenanthrene.² There is a tilted angle δ between two successive benzene rings with respect to each other, and it reaches the extent of 9.5–

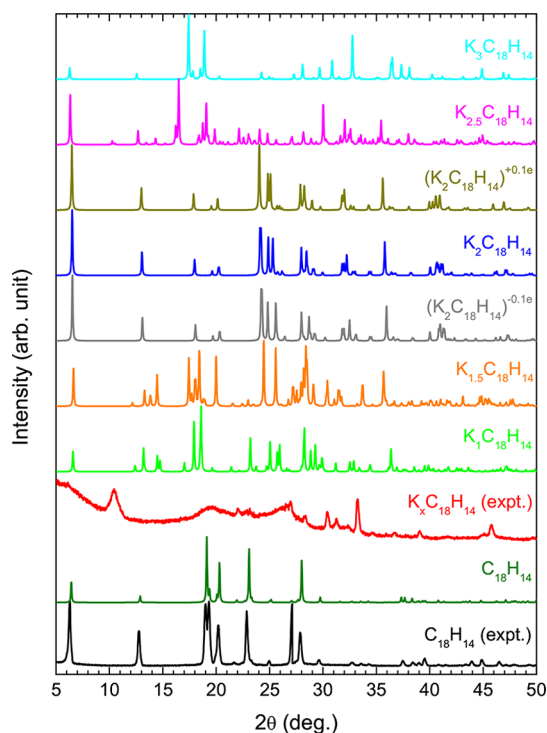


Figure 1. Calculated XRD spectra of pristine and K-doped $C_{18}H_{14}$ compared with the experiments.²² The experimental XRD patterns of K-doped $C_{18}H_{14}$ were taken from the sample with $T_c = 7.2$ K. All XRD data were collected by using the incident wavelength $\lambda = 1.5406$ Å.

10.6° . In addition, viewing from the c direction, K atom is localized on the C–C bond connected benzene ring-1 with ring-2 and closer to ring-1. Scanning the fine-bonding feature, we have found that the C–C bonds linked to two benzene rings (hereafter call them as bridge bonds) are shortened to 1.46 Å from 1.49 Å, whereas the C–C bonds near the bridge bond within the rings become long when one K atom is doped for every organic molecule. The variations of C–C bonds indicate that the charge is not the uniform distribution when transferring to π orbital from the K atom.

For $K_2C_{18}H_{14}$, the herringbone structure is still existent, as shown in Figure 2b. However, three benzene rings in organic molecule are almost coplanar. The tilted angle δ is only 0.2 – 0.6° . Along the b direction, two K atoms are between two organic molecular layers, and viewing from the c direction, K atom lies on the bridge bond. In $K_2C_{18}H_{14}$, the bridge bonds further shorten to 1.44 Å, and the C–C bonds near the bridge bond within the rings become longer. The distinguish of C–C bond lengths within the same ring becomes big which implies a stronger molecular distortion in $K_2C_{18}H_{14}$. Doping three K atoms into solid p -terphenyl, $K_3C_{18}H_{14}$, the system keeps the $P2_1/c$ symmetry, but great changes have taken place in the

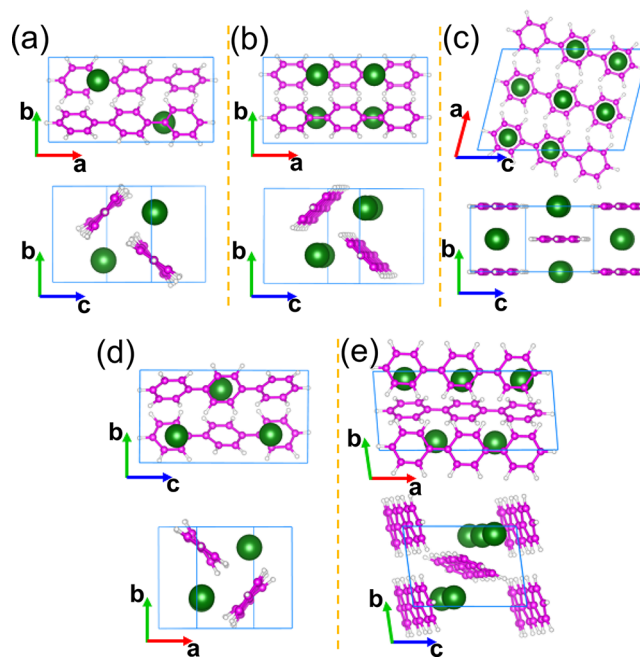


Figure 2. Optimized structures of $K_xC_{18}H_{14}$ viewing from different directions. Pink, white, and green balls represent C, H, and K atoms, respectively. (a) $K_1C_{18}H_{14}$, (b) $K_2C_{18}H_{14}$, (c) $K_3C_{18}H_{14}$, (d) $K_{1.5}C_{18}H_{14}$, and (e) $K_{2.5}C_{18}H_{14}$.

structure, as shown in Figure 2c. All organic molecules rotate and form a visible two-dimensional-layered structure. Along the b direction, three K atoms are all between two organic molecular layers, but viewing from the a direction, K atoms and p -terphenyl molecules are coplanar. Viewing from the b direction, the K atom is on the center of the benzene ring. The varying tendency of C–C bond lengths in $K_3C_{18}H_{14}$ is similar to $K_1C_{18}H_{14}$ and $K_2C_{18}H_{14}$. The bridge bonds further shorten to 1.43 Å.

To identify the observed superconducting phase in experiment, we have analyzed the XRD result. Comparing the experimental XRD between $C_{18}H_{14}$ and $K_xC_{18}H_{14}$ with 7.2 K superconductivity, the abnormal peaks around $2\theta = 10.4^\circ$ and $2\theta = 33.2^\circ$ imply the formation of new phase and a possible phase transition after doping. Additionally, the wide XRD peaks indicate that the crystallinity of the sample is not very good such that the mixture phase can exist. Our calculated XRD of $K_1C_{18}H_{14}$, $K_2C_{18}H_{14}$, and $K_3C_{18}H_{14}$ are presented in Figure 1. Unfortunately, we found that none of the three structures is completely consistent with the experiment in the XRD spectrum. Although the XRD of $K_2C_{18}H_{14}$ or $K_3C_{18}H_{14}$ is closer to the experimental result, the XRD peak around $2\theta = 10.4^\circ$ has not observed in these two pure phases. Thus, we further investigated the possibility of other doped phases. On the one hand, we added a small charge fluctuation into

Table 2. Optimized Crystal Lattice Constants a , b , c , the Angle β between Two Axes, the Tilted Angle δ between Two Successive Benzene Rings with Respect to Each Other and the Volume of Unit Cell V for Every Doping Level

system	space-group	a (Å)	b (Å)	c (Å)	α ($^\circ$)	β ($^\circ$)	γ ($^\circ$)	δ ($^\circ$)	V (Å ³)
$K_1C_{18}H_{14}$	$P2_1$	13.500	6.863	7.181	90	83.12	90	9.5–10.6	660.6
$K_{1.5}C_{18}H_{14}$	$P1$	7.110	7.274	14.743	89.76	64.56	90.02	17.2–20.3	688.6
$K_2C_{18}H_{14}$	$P2_1$	14.001	7.032	7.151	90	75.54	90	0.2–0.6	681.8
$K_{2.5}C_{18}H_{14}$	$P1$	14.585	6.278	9.058	99.25	73.54	96.77	1.1–2.5	782.7
$K_3C_{18}H_{14}$	$P2_1/c$	14.503	5.463	10.243	90	76.13	90	0	787.8

$K_2C_{18}H_{14}$ to form a defect state, such as $(K_2C_{18}H_{14})^{+0.1e}$ and $(K_2C_{18}H_{14})^{-0.1e}$. However, except for the small shift of peaks, this did not change the XRD spectrum in nature, as shown in Figure 1. On the other hand, in the unit cell of K-doped *p*-terphenyl containing two organic molecules, by setting the space group of doped structure as *P1* and respectively doping three and five K atoms into the unit cell, we considered the fractional situations for the doping concentration, such as $K_{1.5}C_{18}H_{14}$ and $K_{2.5}C_{18}H_{14}$, which can also be understood as a mixed phase. In experiment, $K_{1.5}C_{18}H_{14}$ may be obtained by mixing $K_1C_{18}H_{14}$ and $K_2C_{18}H_{14}$, whereas $K_{2.5}C_{18}H_{14}$ can be formed by mixing $K_2C_{18}H_{14}$ and $K_3C_{18}H_{14}$. By subtracting and adding K atoms from/into $K_2C_{18}H_{14}$, we have simply simulated the fractional doping levels in this calculation. Table 2 and Figure 2 present the optimized crystal lattice parameters and geometrical configurations, respectively. Both $K_{1.5}C_{18}H_{14}$ and $K_{2.5}C_{18}H_{14}$ are stabilized at the *P1* symmetry. The volumes of unit cells of doping cases of $x = 1, 1.5, 2, 2.5,$ and 3 do not satisfy the monotonically increasing trend because of the existence of phase transitions during the doping. As shown in Figure 2d, $K_{1.5}C_{18}H_{14}$ is similar to $K_1C_{18}H_{14}$. There are a visible herringbone feature and a big tilted angle between two successive benzene rings with respect to each other. The asymmetric distribution of K atoms in $K_{2.5}C_{18}H_{14}$ (Figure 2e) did not cause the big rotation between two successive benzene rings with respect to each other. However, the arrangement of organic molecules appears more arbitrarily in $K_{2.5}C_{18}H_{14}$. Comparing their XRD with the experiment one in Figure 1, we were surprised to find that $K_{2.5}C_{18}H_{14}$ produced some peak-fitting experiment near $2\theta = 10.4^\circ$ and $2\theta = 33.2^\circ$ and being not observed in $K_{1.5}C_{18}H_{14}$. Of course, the XRD obtained from $K_{2.5}C_{18}H_{14}$ cannot completely match that of the experiment either. As seen from the XRD result, the superconducting phase observed in the experiment is more similar to a mixed phase by $K_2C_{18}H_{14}$ and $K_3C_{18}H_{14}$.

3.3. Stability. To examine the thermodynamic stability of these considered doping cases, we have calculated the formation energy E_f . The E_f for the doping level x is defined as the function of the chemical potential K, given as follows

$$E_f = E_{\text{doped}} - E_{\text{pristine}} - x\mu_K^{\text{bulk}} - x[\mu_K - \mu_K^{\text{bulk}}] \quad (1)$$

where E_{doped} and E_{pristine} are the total energies of the doped and host crystal, respectively. μ_K^{bulk} can be obtained from the energy per K atom in the K metal with the bcc structure. x is the doping concentration. μ_K is the chemical potential of the K species. $\mu_K = \mu_K^{\text{bulk}}$ means the element is so rich that the pure element phase can be formed. $E_f < 0$ indicates that the doped compound can stably exist. From the calculated formation energy shown in Figure 3, all of the considered doped phases are able to exist as the chemical potential of K satisfying certain conditions. Comparing several doping levels, however, $K_{2.5}C_{18}H_{14}$ is more stable because it has the lower formation energy than other phases in a wide range of chemical potential. This suggests that the experimentally observed superconducting phase of 7.2 K shall be $K_{2.5}C_{18}H_{14}$ or a mixture phase.

3.4. Bonding Character and Charge Transfer. Similar to other PAH superconductors, K-doped *p*-terphenyl possesses the typical feature of the charge-transfer salt. Analyzing the interaction between K atoms and organic molecules, we can observe the clear ionic bonding characteristic. The different charge density $\Delta\rho$ [$\Delta\rho = \rho(K_xC_{18}H_{14}) - \rho(C_{18}H_{14}) - \rho(K_x)$], as shown in Figure 4, graphically depicts the charge transferring

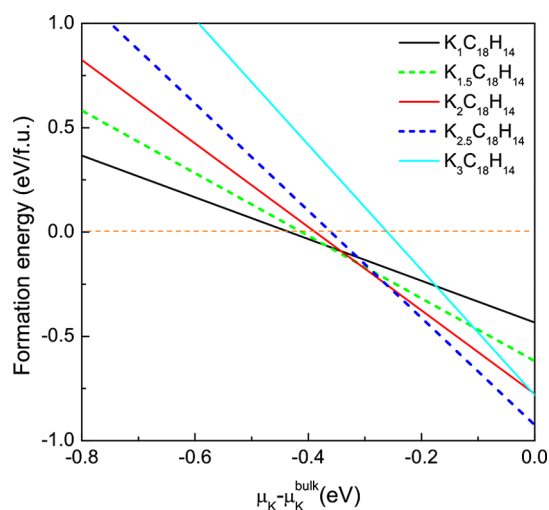


Figure 3. Calculated formation energy of $K_xC_{18}H_{14}$ as a function of the K chemical potential.

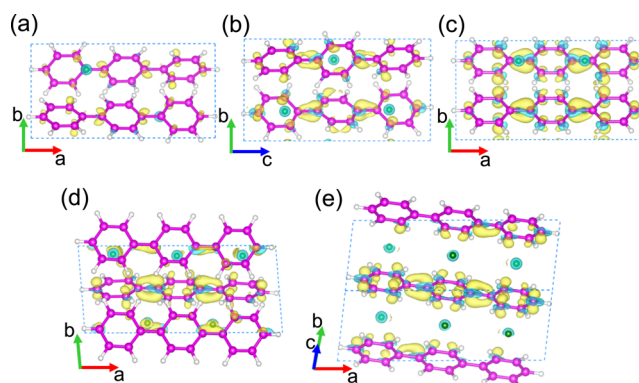


Figure 4. Calculated 3D plots of different charge density for $K_xC_{18}H_{14}$ with the isosurface unit of 5×10^{-3} e/a.u.³. Pink, white, and green balls represent C, H, and K atoms, respectively. The yellow and light blue areas mean the increase and the decrease of electrons in this region, respectively. (a) $K_1C_{18}H_{14}$, (b) $K_{1.5}C_{18}H_{14}$, (c) $K_2C_{18}H_{14}$, (d) $K_{2.5}C_{18}H_{14}$, and (e) $K_3C_{18}H_{14}$.

between K atoms and organic molecules. The yellow and light blue areas define the gain and loss of electrons, respectively. With the increase of the doping content, the quantity of transferred charge is about 0.84, 1.24, 1.65, 1.99, and 2.44 e/f.u. for $K_1C_{18}H_{14}$, $K_{1.5}C_{18}H_{14}$, $K_2C_{18}H_{14}$, $K_{2.5}C_{18}H_{14}$, and $K_3C_{18}H_{14}$, respectively. As mentioned above, the superconducting phase observed by the experiment is predicted as a mixed phase such as the doping level around $x \approx 2.5$. Then, the transferring charge of about two electrons is suggested. Another important information from $\Delta\rho$ is that it visibly shows the distribution of charge transferred to C atoms. As shown in Figure 4, the transferred charge distribution is neither local nor homogeneous. The charge is distributed on part C atoms in a certain symmetrical ordering and highlights the distribution near bridge bonds. As a comparison, the added charge mainly concentrates on the middle benzene ring with the increase of K content. To $K_3C_{18}H_{14}$, the distribution of transferred charge covers all C atoms.

3.5. Electronic Structures. The pristine *p*-terphenyl is a wide-gap semiconductor with the bandgap of 3.3 eV.⁴³ The charge transferring from K atoms to organic molecules makes the Fermi level shift toward higher energy, which results in a

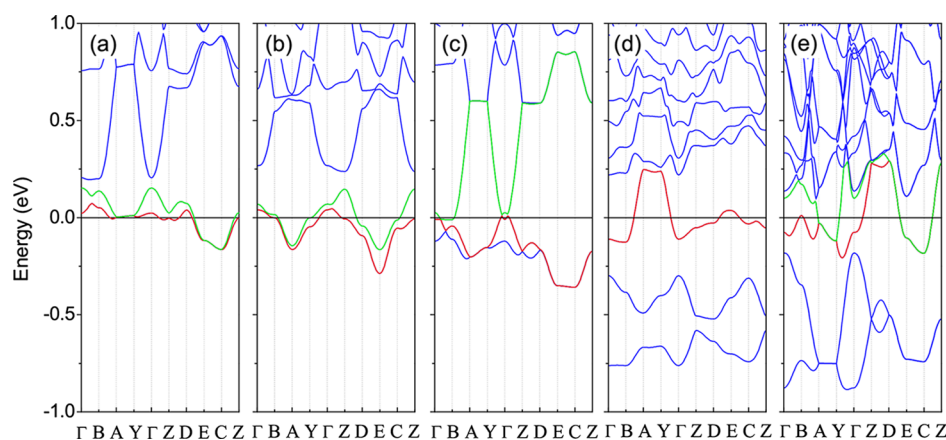


Figure 5. Electronic band structures of $K_xC_{18}H_{14}$ at the NM state. Zero energy denotes the Fermi level. (a) $K_1C_{18}H_{14}$, (b) $K_{1.5}C_{18}H_{14}$, (c) $K_2C_{18}H_{14}$, (d) $K_{2.5}C_{18}H_{14}$, and (e) $K_3C_{18}H_{14}$.

transition from insulator to metal. Figures 5 and 6, respectively, show the band structure and the total density of states (DOS)

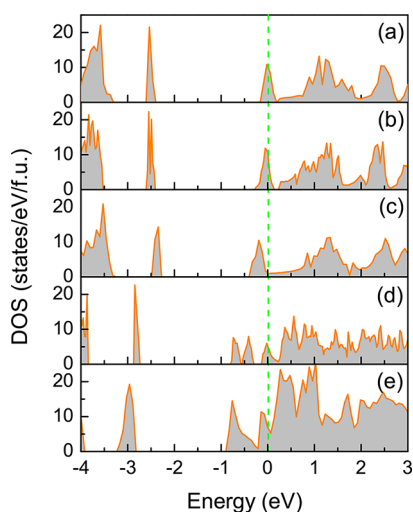


Figure 6. Electronic DOS of $K_xC_{18}H_{14}$ at the NM state. Zero energy denotes the Fermi level. (a) $K_1C_{18}H_{14}$, (b) $K_{1.5}C_{18}H_{14}$, (c) $K_2C_{18}H_{14}$, (d) $K_{2.5}C_{18}H_{14}$, and (e) $K_3C_{18}H_{14}$.

for each doping level at nonmagnetic (NM) state. To make it easier to compare different doping situations, we selected the same k points to form the band path in the reciprocal space. The k points shown in Figure 5 are Γ (0, 0, 0), B (0.5, 0, 0), A (0.5, 0, 0), Y (0, 0.5, 0), Z (0, 0, 0.5), D (0.5, 0, 0.5), E (0.5, 0.5, 0.5), and C (0, 0.5, 0.5), respectively. Under $P2_1$ symmetry, the conjugated molecules split each orbital into a pair of partly degenerate bands in $K_1C_{18}H_{14}$. As shown in Figure 5a, two partly degenerate bands forming the first group conduction band cross the Fermi level. However, transforming to $K_{1.5}C_{18}H_{14}$ with $P1$ symmetry (Figure 5b), the coupling between the two conjugated molecules is weakened, which leads to a bigger splitting of bands. These former two doping levels both drive the high DOS at the Fermi level (N_{E_F}), as shown in Figure 6a,b. The values of N_{E_F} are 10.25 and 10.43 states/eV/f.u. for $K_1C_{18}H_{14}$ and $K_{1.5}C_{18}H_{14}$, respectively. More electrons transferring to organic molecules, in $K_2C_{18}H_{14}$, as shown in Figure 5c, the Fermi level moves into the overlap region of two group of conduction bands formed by two

molecular orbitals. $K_2C_{18}H_{14}$ exhibits the weak metallic feature with a small N_{E_F} value of 1.28 states/eV/f.u., as shown in Figure 6c. In $K_{2.5}C_{18}H_{14}$ (Figure 5d), more electrons transferring to organic molecules rise the Fermi level into the second group of conduction band. However, the conjugated character of the organic molecules completely disappears, which further weakens the coupling among bands. One band crosses the Fermi level, differing from the two-band model in other doping cases. The Fermi level is localized at a DOS peak (Figure 6d) which results in a slightly big N_{E_F} value of 5.1 states/eV/f.u. For $K_3C_{18}H_{14}$ with $P2_1/c$ symmetry, as shown in Figure 5e, the Fermi level moves into the second group of conduction band. The interactions between K atoms and molecules strengthen, which makes the bands become more extended. As shown in Figure 6e, a stronger metallic feature (3.57 states/eV/f.u. for N_{E_F}) is observed in $K_3C_{18}H_{14}$ than in $K_2C_{18}H_{14}$. The result of electronic structures also indicates that we can obtain higher N_{E_F} value by tuning the chemical potential of K to realize the high superconductivity, which is consistent with Mazziotti's suggestion.⁴⁴

Previous studies have pointed out that the doped PAHs are often at the AFM ground state.^{10–13} Hence, we have investigated the magnetism of K-doped p -terphenyl. It was found that both $K_1C_{18}H_{14}$ and $K_{1.5}C_{18}H_{14}$ are at the AFM ground state. The total energy of the AFM state is respectively 40.4 meV for $K_1C_{18}H_{14}$ and 9.2 meV for $K_{1.5}C_{18}H_{14}$ less than that of their NM state. The local magnetic moments are 0.57 and 0.22 μ_B /f.u. for $K_1C_{18}H_{14}$ and $K_{1.5}C_{18}H_{14}$, respectively. The electronic states at the Fermi level, as shown in Figure 7, visibly decrease, and the values of N_{E_F} reduce to 1.6 and 5.5 states/eV/f.u. for $K_1C_{18}H_{14}$ and $K_{1.5}C_{18}H_{14}$, respectively. Interestingly, all of $K_2C_{18}H_{14}$, $K_{2.5}C_{18}H_{14}$, and $K_3C_{18}H_{14}$ are stabilized at the NM state. Comparing these magnetic structures in K-doped p -terphenyl, the difference of magnetism possibly results from the distortion in organic molecular plane. As shown in Figure 2, the tilt between two successive benzene rings drives the spin ordering of electrons transferred to C atoms from K atoms. With the increase of charge transferring, the spin ordering disappears in systems while the superconductivity occurs.

3.6. Discussions. With regard to the superconductivity of K-doped p -terphenyl, more data and analyses are yet to come. The complexity of the superconducting mechanism in K-doped p -terphenyl is evidenced by the recent reported three critical

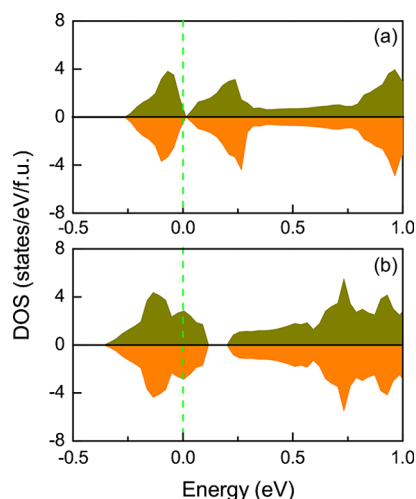


Figure 7. Electronic DOS of $K_1C_{18}H_{14}$ (a) and $K_{1.5}C_{18}H_{14}$ (b) with the AFM spin polarization. Zero energy denotes the Fermi level.

temperatures, 7.2, 43, and 123 K, in the same material.^{22–24} In previous studies, however, we have pointed out that there is a common phase to show T_c in the range of $5 < T_c < 7$ K in all K-doped aromatic compounds.⁹ The existed superconductivity of 7.2 K in K-doped *p*-terphenyl just confirms that prediction. For this low T_c phase, the electron–phonon coupling mechanism is enough to describe this superconductivity. From previous investigations,^{9,45} the phonons with low and middle frequencies mainly contribute to the electron–phonon interaction. The maximum value of our calculated middle frequency of $K_2C_{18}H_{14}$ is about 1574 cm^{-1} , which is almost equal to that of the K-doped picene⁴⁵ and also comparable with that of $K_2C_6H_6$.⁹ At the same time, the N_{E_F} can change with the doping content around 5.1 states/eV/f.u. for $K_{2+\delta}C_{18}H_{14}$ ($0 < \delta < 1$) because of the charge fluctuations. On the basis of the comparable N_{E_F} of K-doped *p*-terphenyl with K-doped benzene and picene in the range of 4–6 states/eV/f.u.,^{9,45} and combining with the similar feasible screened Coulomb pseudopotential μ^* of 0.1, we can predict that the T_c of K-doped *p*-terphenyl is in the range of $5 < T_c < 7$ K, which is in accordance with the experimental observation.²³ In other words, the observed superconducting phase is a mixed compound in the doping range of $2 < x < 3$ instead of pure $K_1C_{18}H_{14}$ or $K_{1.5}C_{18}H_{14}$ phase, which is just what we predicted by XRD, thermodynamic stability, and electronic and magnetic properties.

With regard to the higher transition temperature, the experimental investigations presented unknown peaks in Raman spectra. These unknown peaks are possibly induced by graphite, C_{60} , and other modes.^{23,24} On the one hand, therefore, we infer that the two higher transition temperatures may be from other new superconducting modes such as CK_x , KH_x , and $K-CH_x$ compounds induced by the reconstruction. On the other hand, as in our previous studies,^{9,19} some internal and external factors can be the cause of high superconducting transition temperature, such as electronic correlations and pressure. The strong electronic correlations in K-doped *p*-terphenyl were implied by Baskaran⁴⁶ and Fabrizio et al.⁴⁷ In this kind of low-dimensional organic system, therefore, the high superconductivity may be related with the electronic correlational effects. To clarify the matter, more efforts in the future are surely needed.

4. CONCLUSIONS

In conclusion, with the aim of exploring the structural and bonding characteristics of K-doped *p*-terphenyl which has been discovered to be a superconductor with $T_c = 7.2\text{--}123$ K, we have carried out the first-principles calculations based on the vdW-DF2 functional. Considering five doping levels of $x = 1, 1.5, 2, 2.5,$ and 3 in $K_xC_{18}H_{14}$, we have predicted the optimized crystal structures at each doping level, calculated the XRD spectra, and investigated the thermodynamic stability, ionic bonding characteristics, charge transfer, and electronic and magnetic properties. All of these five doping phases are able to exist in the experiment based on the negative formation energy, but $K_{2.5}C_{18}H_{14}$ or say a mixed phase by $K_2C_{18}H_{14}$ and $K_3C_{18}H_{14}$ is more stable in a wide range of chemical potential. The XRD summarized by $K_2C_{18}H_{14}$, $K_{2.5}C_{18}H_{14}$, and $K_3C_{18}H_{14}$ can almost match that of experiment. The charge transfer from K atoms to organic molecules results in the insulator–metal transition. However, both $K_1C_{18}H_{14}$ and $K_{1.5}C_{18}H_{14}$ are stabilized at the AFM ground state, whereas the latter three compounds exhibit the nonmagnetic behavior. The superconducting phase observed in experiment should be a mixture phase with a doping level in the range of $2 < x < 3$. However, the multifermionity of band structures near the Fermi level indicates that the driving force for superconductivity is complicated. Future works are needed to understand the superconductivity, especially for the transition temperature above 40 K.

■ ASSOCIATED CONTENT

Supporting Information

The Supporting Information is available free of charge on the ACS Publications website at DOI: 10.1021/acs.jpcc.7b12616.

Optimized structures of K-doped *p*-terphenyl ($K_xC_{18}H_{14}$, $x = 1, 1.5, 2, 2.5,$ and 3) in the format of the cif file (ZIP)

■ AUTHOR INFORMATION

Corresponding Authors

*E-mail: xjchen@hpstar.ac.cn. Phone: +86 (0)10 56981818.

Fax: +86 (0)10 56981818 (X.-J.C.).

*E-mail: haiqing0@csrc.ac.cn (H.-Q.L.).

ORCID

Guo-Hua Zhong: 0000-0003-0673-8738

Chao Zhang: 0000-0002-5957-2287

Notes

The authors declare no competing financial interest.

■ ACKNOWLEDGMENTS

The work was supported by the National Natural Science Foundation of China (grant nos. 61574157 and 61774164) and the Basic Research Program of Shenzhen (grant nos. JCYJ20160331193059332, JCYJ20150529143500956, and JCYJ20150401145529035). H.Q.L., X.H.W., J.X.H., and G.H.Z. acknowledge support from NSAF U1530401 and computational resource from the Beijing Computational Science Research Center. The partial calculation was supported by the Special Program for Applied Research on Super Computation of the NSFC-Guangdong Joint Fund (the second phase) under grant no. U1501501.

■ REFERENCES

(1) Mitsuhashi, R.; Suzuki, Y.; Yamanari, Y.; Mitamura, H.; Kambe, T.; Ikeda, N.; Okamoto, H.; Fujiwara, A.; Yamaji, M.; Kawasaki, N.;

- Maniwa, Y.; Kubozono, Y. Superconductivity in Alkali-Metal-Doped Picene. *Nature* **2010**, *464*, 76–79.
- (2) Wang, X. F.; Liu, R. H.; Gui, Z.; Xie, Y. L.; Yan, Y. J.; Ying, J. J.; Luo, X. G.; Chen, X. H. Superconductivity at 5 K in Alkali-Metal-Doped Phenanthrene. *Nat. Commun.* **2011**, *2*, 507.
- (3) Wang, X. F.; Yan, Y. J.; Gui, Z.; Liu, R. H.; Ying, J. J.; Luo, X. G.; Chen, X. H. Superconductivity in $A_{1.5}$ phenanthrene ($A = \text{Sr, Ba}$). *Phys. Rev. B: Condens. Matter Mater. Phys.* **2011**, *84*, 214523.
- (4) Wang, X. F.; Luo, X. G.; Ying, J. J.; Xiang, Z. J.; Zhang, S. L.; Zhang, R. R.; Zhang, Y. H.; Yan, Y. J.; Wang, A. F.; Cheng, P.; Ye, G. J.; Chen, X. H. Enhanced Superconductivity by Rare-Earth Metal Doping in Phenanthrene. *J. Phys.: Condens. Matter* **2012**, *24*, 345701.
- (5) Artioli, G. A.; Hammerath, F.; Mozzati, M. C.; Carretta, P.; Corana, F.; Mannucci, B.; Margadonna, S.; Malavasi, L. Superconductivity in Sm-doped $[n]$ Phenacenes ($n = 3, 4, 5$). *Chem. Commun.* **2015**, *51*, 1092–1095.
- (6) Kubozono, Y.; Goto, H.; Jabuchi, T.; Yokoya, T.; Kambe, T.; Sakai, Y.; Izumi, M.; Zheng, L.; Hamao, S.; Nguyen, H. L. T.; Sakata, M.; Kagayama, T.; Shimizu, K. Superconductivity in Aromatic Hydrocarbons. *Physica C* **2015**, *514*, 199–205.
- (7) Kubozono, Y.; Mitamura, H.; Lee, X.; He, X.; Yamanari, Y.; Takahashi, Y.; Suzuki, Y.; Kaji, Y.; Eguchi, R.; Akaike, K.; Kambe, T.; Okamoto, H.; Fujiwara, A.; Kato, T.; Kosugi, T.; Aoki, H. Metal-Intercalated Aromatic Hydrocarbons: A New Class of Carbon-Based Superconductors. *Phys. Chem. Chem. Phys.* **2011**, *13*, 16476–16493.
- (8) Xue, M.; Cao, T.; Wang, D.; Wu, Y.; Yang, H.; Dong, X.; He, J.; Li, F.; Chen, G. F. Superconductivity Above 30 K in Alkali-Metal Doped Hydrocarbon. *Sci. Rep.* **2012**, *2*, 389.
- (9) Zhong, G.; Chen, X.-J.; Lin, H.-Q. Prediction of Superconductivity in Potassium-Doped Benzene. 2015, arXiv:1501.00240. arXiv.org e-Print archive. <http://lanl.arxiv.org/abs/1501.00240> (accessed Jan 1, 2015).
- (10) Zhong, G.-H.; Zhang, C.; Wu, G.-F.; Huang, Z.-B.; Chen, X.-J.; Lin, H.-Q. First-Principles Investigations on the Magnetic Property in Tripotassium Doped Picene. *J. Appl. Phys.* **2013**, *113*, 17E131.
- (11) Zhong, G.; Huang, Z.; Lin, H. Antiferromagnetism in Potassium-Doped Polycyclic Aromatic Hydrocarbons. *IEEE Trans. Magn.* **2014**, *50*, 1700103.
- (12) Yan, X.-W.; Wang, Y.; Gao, M.; Ma, D.; Huang, Z. Magnetic and Electronic Properties of Samarium-Doped Phenanthrene from First-Principles Study. *J. Phys. Chem. C* **2016**, *120*, 22565–22570.
- (13) Giovannetti, G.; Capone, M. Electronic Correlation Effects in Superconducting Picene from Ab Initio Calculations. *Phys. Rev. B: Condens. Matter Mater. Phys.* **2011**, *83*, 134508.
- (14) Kim, M.; Min, B. I.; Lee, G.; Kwon, H. J.; Rhee, Y. M.; Shim, J. H. Density Functional Calculations of Electronic Structure and Magnetic Properties of the Hydrocarbon K_3 picene Superconductor Near the Metal-Insulator Transition. *Phys. Rev. B: Condens. Matter Mater. Phys.* **2011**, *83*, 214510.
- (15) Huang, Z.; Zhang, C.; Lin, H.-Q. Magnetic Instability and Pair Binding in Aromatic Hydrocarbon Superconductors. *Sci. Rep.* **2012**, *2*, 922.
- (16) Ruff, A.; Sing, M.; Claessen, R.; Lee, H.; Tomić, M.; Jeschke, H. O.; Valentí, R. Absence of Metallicity in K-Doped Picene: Importance of Electronic Correlations. *Phys. Rev. Lett.* **2013**, *110*, 216403.
- (17) Han, J.-X.; Zhong, G.-H.; Wang, X.-H.; Chen, X.-J.; Lin, H.-Q. The First-Principles Investigations on Magnetic Ground-State in Sm-Doped Phenanthrene. *AIP Adv.* **2017**, *7*, 055704.
- (18) Wang, X.-H.; Zhong, G.-H.; Han, J.-X.; Chen, X.-J.; Lin, H.-Q. Structural and Antiferromagnetic Properties of Sm-Doped Chrysene. *AIP Adv.* **2017**, *7*, 055707.
- (19) Zhong, G.-H.; Yang, C.-L.; Chen, X.-J.; Lin, H.-Q. Superconductivity in Solid Benzene Molecular Crystal. 2016, arXiv:1612.01217. arXiv.org e-Print archive. <http://lanl.arxiv.org/abs/1612.01217> (accessed Dec 5, 2016).
- (20) Little, W. A. Possibility of Synthesizing an Organic Superconductor. *Phys. Rev. A* **1964**, *134*, A1416–A1424.
- (21) Ginzburg, V. L. High-Temperature Superconductivity-Dream or Reality? *Sov. Phys. Usp.* **1976**, *19*, 174–179.
- (22) Wang, R.-S.; Gao, Y.; Huang, Z.-B.; Chen, X.-J. Superconductivity in *p*-Terphenyl. 2017, arXiv:1703.05803. arXiv.org e-Print archive. <http://lanl.arxiv.org/abs/1703.05803> (accessed Mar 16, 2017).
- (23) Wang, R.-S.; Gao, Y.; Huang, Z.-B.; Chen, X.-J. Superconductivity at 43 K in a Single C-C Bond Linked Terphenyl. 2017, arXiv:1703.05804. arXiv.org e-Print archive. <http://lanl.arxiv.org/abs/1703.05804> (accessed Mar 16, 2017).
- (24) Wang, R.-S.; Gao, Y.; Huang, Z.-B.; Chen, X.-J. Superconductivity Above 120 Kelvin in a Chain Link Molecule. 2017, arXiv:1703.06641. arXiv.org e-Print archive. <http://lanl.arxiv.org/abs/1703.06641> (accessed Mar 20, 2017).
- (25) Gao, Y.; Wang, R.-S.; Wu, X.-L.; Cheng, J.; Deng, T.-G.; Yan, X.-W.; Huang, Z.-B. Searching Superconductivity in Potassium-Doped *p*-Terphenyl. *Acta Phys. Sin.* **2016**, *65*, 077402.
- (26) Li, H.; Zhou, X.; Parham, S.; Nummy, T.; Griffith, J.; Gordon, K.; Chronister, E. L.; Dessau, D. S. Spectroscopic Evidence of Pairing Gaps to 60 Kelvin or Above in Surface-Doped *p*-Terphenyl Crystals. 2017, arXiv:1704.04230. arXiv.org e-Print archive. <http://lanl.arxiv.org/abs/1704.04230> (accessed Apr 13, 2017).
- (27) Liu, W.; Lin, H.; Kang, R.; Zhu, X.; Zhang, Y.; Zheng, S.; Wen, H.-H. Magnetization of Potassium-doped *p*-Terphenyl and *p*-Quaterphenyl by High-Pressure Synthesis. *Phys. Rev. B* **2017**, *96*, 224501.
- (28) Baudour, J. L.; Delugeard, Y.; Cailleau, H. Transition Structurale Dans Les Polyphenyles. I. Structure Cristalline de la Phase Basse Temperature du *p*-Terphenyle 113 K. *Acta Crystallogr., Sect. B: Struct. Crystallogr. Cryst. Chem.* **1976**, *32*, 150–154.
- (29) Baudour, J. L.; Cailleau, H.; Yelon, W. B. Structural Phase Transition in Polyphenyls. IV. Double-Well Potential in the Disordered Phase of *p*-Terphenyl from Neutron (200 K) and X-Ray (Room-Temperature) Diffraction Data. *Acta Crystallogr., Sect. B: Struct. Crystallogr. Cryst. Chem.* **1977**, *33*, 1773–1780.
- (30) Liu, T.; Xu, S.; Sun, C.; Zhou, M. Raman Spectroscopic Studies on *p*-Terphenyl Under High Pressure. *Chem. Phys. Lett.* **2014**, *615*, 1–5.
- (31) Kresse, G.; Furthmüller, J. Efficiency of Ab-Initio Total Energy Calculations for Metals and Semiconductors Using a Plane-Wave Basis Set. *Comput. Mater. Sci.* **1996**, *6*, 15–50.
- (32) Kresse, G.; Furthmüller, J. Efficient Iterative Schemes for Ab Initio Total-Energy Calculations Using a Plane-Wave Basis Set. *Phys. Rev. B: Condens. Matter Mater. Phys.* **1996**, *54*, 11169–11186.
- (33) Perdew, J. P.; Burke, K.; Ernzerhof, M. Generalized Gradient Approximation Made Simple. *Phys. Rev. Lett.* **1996**, *77*, 3865.
- (34) Lee, K.; Murray, É. D.; Kong, L.; Lundqvist, B. I.; Langreth, D. C. Higher-Accuracy van der Waals Density Functional. *Phys. Rev. B: Condens. Matter Mater. Phys.* **2010**, *82*, No. 081101(R).
- (35) Zhong, G.-H.; Zhang, C.; Yan, X.; Li, X.; Du, Z.; Jing, G.; Ma, C. Structural and Electronic Properties of Potassium Doped 1,2,8,9-Dibenzopentacene Superconductor: Comparing with Doped [7]-Phenacenes. *Mol. Phys.* **2017**, *115*, 472.
- (36) Wang, X.; Zhong, G.; Yan, X.; Chen, X.; Lin, H. First-Principles Prediction on Geometrical and Electronic Properties of K-Doped Chrysene. *J. Phys. Chem. Solids* **2017**, *104*, 56.
- (37) Rietveld, H. M.; Maslen, E. N.; Clews, C. J. B. An X-Ray and Neutron Diffraction Refinement of the Structure of *p*-Terphenyl. *Acta Crystallogr., Sect. B: Struct. Crystallogr. Cryst. Chem.* **1970**, *26*, 693–706.
- (38) Saitoh, H.; Saito, K.; Yamamura, Y.; Matsuyama, H.; Kikuchi, K.; Iyoda, M.; Ikemoto, I. Crystal Structures of the Room-Temperature Phase of 4,4''-Difluoro-*p*-Terphenyl and 4,4'''-Difluoro-*p*-Quaterphenyl. *Bull. Chem. Soc. Jpn.* **1993**, *66*, 2847–2853.
- (39) Puschign, P.; Heimel, G.; Weinmeier, K.; Resel, R.; Ambrosch-Draxl, C. High Pressure Studies on the Optical and Electronic Properties of *Para*-Terphenyl. *High Pressure Res.* **2002**, *22*, 105–109.
- (40) Murugan, N. A.; Yashonath, S. Pressure Induced Orientational Ordering in *p*-Terphenyl. *J. Phys. Chem. B* **2005**, *109*, 1433–1440.
- (41) Selvakumar, S.; Sivaji, K.; Balamurugan, N.; Arulchakkaravarthi, A.; Sankar, S.; Venkateswaran, C.; Ramasamy, P. Growth and Studies

on SSVBT Grown *p*-Terphenyl Single Crystals. *J. Cryst. Growth* **2005**, *275*, e265–e271.

(42) Ceperley, D. M.; Alder, B. J. Ground State of the Electron Gas by a Stochastic Method. *Phys. Rev. Lett.* **1980**, *45*, 566.

(43) Yoshino, K.; Hirohata, M.; Tada, K.; Fujii, A.; Ozaki, M.; Naka, A.; Ishikawa, M. Optical Properties of Poly[(disilanylene)-oligophenylenes]. *Proc. SPIE* **1997**, *3145*, 192–199.

(44) Mazziotti, M. V.; Valletta, A.; Campi, G.; Innocenti, D.; Perali, A.; Bianconi, A. Possible Fano resonance for High- T_c Multi-Gap Superconductivity in *p*-Terphenyl Doped by K at the Lifshitz Transition. *Europhys. Lett.* **2017**, *118*, 37003.

(45) Casula, M.; Calandra, M.; Profeta, G.; Mauri, F. Intercalant and Intermolecular Phonon Assisted Superconductivity in K-Doped Picene. *Phys. Rev. Lett.* **2011**, *107*, 137006.

(46) Baskaran, G. Two Mott Insulator Theory of Superconductivity in K_3X (X : Picene, *p*-Terphenyl, C60). 2017, arXiv:1704.08153. arXiv.org e-Print archive. <http://lanl.arxiv.org/abs/1704.08153> (accessed Apr 26, 2017).

(47) Fabrizio, M.; Qin, T.; Naghavi, S. S.; Tosatti, E. Two-Band s_{\pm} Strongly Correlated Superconductivity in K_3 *p*-Terphenyl? 2017, arXiv:1705.05066. arXiv.org e-Print archive. <http://lanl.arxiv.org/abs/1705.05066> (accessed May 15, 2017).